Experiments in Fluids 29 (2000) 184–197 © Springer-Verlag 2000

An advanced off-axis holographic particle image velocimetry (HPIV) system

Ye Pu, H. Meng

Abstract Holographic PIV (HPIV) is the most promising candidate for the next generation full-field velocimetry that can measure high spatial resolution instantaneous three-dimensional (3D) velocity fields. To explore the maximum performance capabilities of HPIV including spatial resolution, off-axis holography based HPIV has become a major direction of development. A fully automated off-axis HPIV system based on an injection-seeded dual-pulsed YAG laser and 3D data processing software has been implemented in the laser flow diagnostics lab (LFD). In our system, 90-degree particle scattering, dual reference beams, in situ reconstruction/data processing, and 3D velocity extraction based on a fast "concise cross correlation" (CCC) algorithm are utilized. The off-axis HPIV system is tested for an acoustically excited air jet and the wake of a surface-mounted tab in a water channel flow, giving instantaneous 3D velocity fields for both flows. Experimental data of instantaneously measured 3D flow structures using this technique show great promise.

1 Introduction

Over the past decade particle image velocimetry (PIV), which measures two components of velocity in a 2D plane based on photographic imaging, has become the state-of-the-art experimental technique for fluid velocity measurement (Adrian 1991). It employs laser light sheets and planar imaging media (e.g. photographic films or video CCD cameras) to measure the two in-plane components of fluid velocities in a planar domain in a flow, or three components in a planar domain if a stereoscopic imaging technique is used (Arroyo and Greated 1991; Prasad and Adrian 1993). The establishment of PIV clearly marks a significant advancement in experimental fluid mechanics from single-point to multi-point velocity measurement (Adrian 1996; Adrian 1997). This progress, however, is only half way towards full-field three-dimensional (3D) measurement of turbulent flows, and by far the easier half. Attempts have been made to generalize these 2D planar PIV techniques into 3D volumetric field measurement through scanning (Guezennec et al. 1994; Bruecker 1995; Bruecker 1997) with severe limitations in spatial and temporal resolutions. Hence, planar PIV techniques are unable to provide detailed space- and time-resolved experimental data in highly transient and three-dimensional turbulent flows needed for understanding, modeling and controlling of turbulent flows.

Recent advancements in both experimental and computational fluid dynamics research has increased the demand for instantaneous full-field 3D flow velocity measurements resolved in space and time. Measurements of turbulent and complex flows require good accuracy and high resolution in a relatively large volumetric domain. The requirement for information capacity is far beyond any photography-based technique. By capturing the phase information of light waves scattered off the object of interest, holography is an instantaneous 3D imaging process that offers an enormous storage capacity suitable for 3D information recording. It is thus an inherently better solution to 3D measurements than any other available technique. HPIV records the 3D information of a large quantity of particles in a fluid volume on a hologram instantaneously and then reconstructs the particle images in a 3D space. From the reconstructed image field, we can retrieve the 3D positions (as well as size and shape information) of these particles. Furthermore, by finding the 3D displacements of the particles in the image volume between two exposures separated by a short time lapse, the instantaneous 3D velocities of these particles in the volume can also be obtained.

The key problems that any HPIV system faces are reduction of speckle noise, handling of huge quantities of data, extraction of 3D velocity in presence of large gradients/fluctuations, and system complexity vs. user-friend-

Received: *12 August 1998/Accepted*: *20 October 1999*

Ye Pu[1], H. Meng[1]
Laser Flow Diagnostics Laboratory
Mechanical and Nuclear Engineering Department
Kansas State University
Manhattan, KS 66506

[1] *Current address*: SUNY Buffalo, Mechanical and Aerospace Engineering, Buffalo, NY14260

Correspondence to: H. Meng

The authors wish to thank the National Science Foundation for their support through a CAREER Award (CTS-9625307) and a Research Equipment Grant (CTS-9700373), Program Director Mike Roco. We also wish to acknowledge the support from the Air Force Office of Scientific Research and Kansas Program for Complex Fluid Flows. Valuable contributions from Zhijian Huang and Jian Sheng during the course of the HPIV development are greatly appreciated. We also thank Xiangqun Song for suggestions in revision of the manuscript.

liness. While the strategies of handling all these issues make each setup unique, HPIV configurations can be broadly classified into two kinds based on the nature of the holographic scheme: "in-line", where only one beam is employed to produce both the object wave and the reference wave, and "off-axis", where separate object beam and reference beam(s) are introduced. Many variations of these two basic schemes are possible, often blurring such distinctions.

Classical in-line holography (also known as Gabor holography) has been traditionally the standard holographic method to diagnose particle fields (Trolinger et al. 1973; Thompson 1974; Belz and Menzel 1979) and thus was employed in holographic PIV (Weinstein et al. 1985; Meng and Hussain 1991; Scherer and Bernal 1997). While enjoying simplicity of optical geometry and low requirements for laser coherence and energy, standard in-line method, especially when used in HPIV where the particle density is usually large, faces a severe problem. Due to the superposition of the real image, virtual image and reference waves, excessive speckle noise is produced to interfere with recognition of particle images (Meng et al. 1993). Another problem with in-line HPIV that affects the measurement accuracy is the large depth of focus in the reconstructed particle images. This is caused by the small effective numerical aperture (N.A.) formed by the forward particle scattering. Efforts have been made to address these problems to improve the practicality of in-line HPIV while maintaining its merits (Simmons et al. 1993; Zimmin et al. 1993; Zimmin and Hussain 1994; Meng and Hussain 1995a). Among these methods the in-line recording off-axis viewing (IROV) technique appears to be an efficient way to suppress the speckle noise and improve the signal to noise ratio (SNR) of the reconstructed particle images. At the same time, only one beam is used in hologram recording, thus retaining the advantages of in-line HPIV. Holographic PIV based on IROV has been successfully applied to instantaneous 3D flow measurements (Meng and Hussain 1995a, b; Sheng and Meng 1998).

With the innovative IROV approach, in-line HPIV has reached a certain level of applicability. Indeed, its optical simplicity makes it attractive for many applications including holographic 3D flow visualization, and hence it is one of the major HPIV techniques this and other labs are currently pursuing (Sheng and Meng 1998; Meng et al. 1998). However, at a seeding density of no more than a few particles per mm^3, which is a de facto limitation of IROV, the achievable spatial resolution of in-line HPIV is still far from fully resolving turbulent flows. In the pursuit of high spatial resolution measurement, off-axis holography becomes the logical choice. With this scheme, the real, virtual images and the reference beam are no longer superposed, eliminating the major source of speckle noise inherent in in-line HPIV.

2
Rationale of the off-axis HPIV technique

Compared with in-line techniques, off-axis holography tolerates higher seeding densities and offers a much better image SNR, since the directly transmitting wave, the virtual and real image waves are naturally separated during reconstruction. By utilizing wide-spread side scattering rather than the narrow central-lob forward scattering of particles, the effective numerical aperture (N.A.) of imaging is drastically increased, thereby reducing the depth of focus and yielding higher measurement accuracy. Also the directional ambiguity problem inherent in double-exposure in-line HPIV can be solved by employing dual reference waves at different angles. These make off-axis HPIV a desirable configuration despite the optical complexities and the high requirements on the laser power and coherence. However, the particle scattering characteristics require a trade-off between the achievable effective N.A. and the laser energy utilization, since most of the laser energy scattered by the particles is carried by the narrow-angled forward scattering. Side scattering is much weaker than forward scattering and near-forward scattering, thus calling for much higher laser power/energy than what in-line versions require.

Various off-axis methods have been proposed and reported since the early years of HPIV development (Barnhart et al. 1994; Meng 1994; Liu and Hussain 1995; Zhang et al. 1997), addressing the problem of laser energy utilization and effective N.A. Encouraged by the high scattering efficiency of the forward scattering, Zhang et al. (1997) constructed a hybrid HPIV system, where forward scattering is combined with off-axis holography. In the configuration an optical high-pass spatial filter is utilized to avoid the directly transmitting wave in the object beam. In contrast, Barnhart et al. (1994) implemented a phase conjugate HPIV system, where two separate channels of near-forward scattering are combined to achieve an effective large N.A. of particle images. To compensate for the severe optical distortion and aberration imposed by the complex optics, a phase conjugate reconstruction system is required. These two approaches exemplify compromises between the laser energy utilization and the effective N.A.

Such compromises in off-axis HPIV often come with undesirable problems. In the system of Zhang et al. (1997) the employment of the central-lob forward scattering and long recording distance results in low effective N.A. To make up for the large depth of focus, an extra hologram has to be placed in the orthogonal axis to provide velocity component in depth direction. Such a system involves not only doubling the amount of optics and data processing, strict coordination of the two orthogonal holograms, and synthesis of 3D vector map, but also requires the flow domain to be optically accessible from two orthogonal directions through four windows. On the other hand, the phase-conjugate off-axis HPIV system by Barnhart et al. (1994) involves a different type of practical restriction. In spite of the low *f*-number lenses, the two-channel optical system used for collecting scattering works effectively as a low-quality imaging system, introducing excessive optical aberrations that prohibit the reconstruction of particle images. The only remedy is to employ the so-called phase-conjugate reconstruction, i.e. extract back tracing of optical waves from the hologram to the particle images. This requires placing everything, including the original flow medium and its wall, that appeared between the particles and the hologram during the recording, back into the

reconstruction system. Often, this is not feasible, and when it is feasible (as in the case of an open jet in air with no walls), extremely strict alignment of hologram and optics is necessary. In addition, both these off-axis HPIV systems described above resort to the use of a separate laser (a continuous-wave laser) for hologram reconstruction. Since misalignment and difference in wavefronts are inevitable, switching lasers introduces additional sources of image distortion and noise. Furthermore, when the recording and reconstruction lasers do not share the same wavelength, as with the approach of Zhang et al. (1997), extra image aberration is generated from the wavelength difference.

Among the practical obstacles in HPIV application noise is the most critical issue. While the use of off-axis holography eliminates the excessive speckle noise specially associated with in-line holography (Meng et al. 1993), other types of noise still exist, among which the superposition of reconstructed particle images in a volumetric region is the most prominent. This is because the light flux from those out-of-focus particle images in the real image field entering the pupil of the objective lens – although not imaged – can form a speckle noise background. Such noise increases with the particle seeding density and the depth of the image volume. The contribution of particle images far from the focal plane is a low-intensity, homogeneous white noise, and we denote it as trivial noise. In contrast, the contribution of particle images slightly out of focus is a localized high-intensity noise, and we denote it as critical noise. It is indicated that the increase of effective N.A. has different effects on these two kinds of noises. The trivial noise increases with increasing effective N.A. However, it can be filtered out easily, since its image characteristics including power spectrum is quite different from those of the effective image signal. On the other hand, the critical noise decreases with increasing effective N.A., because the image depth of focus becomes shorter, resulting in less image overlap. Since the critical noise is much harder to eliminate due to its similarity in characteristics to the effective image signal, an increase in effective N.A. improves the overall image quality.

On these considerations, we propose a different solution than the past approaches to the off-axis HPIV. A high effective N.A. is achieved by using 90-degree scattering, which provides homogeneous intensity distribution over a large solid angle (Meng 1994), and by shortening the recording distance without adding any optics between the hologram and the particle field. The optical configuration of the 90-degree scattering HPIV resembles that of planar PIV to a large degree in that the flow facility is illuminated from one direction and imaged from an orthogonal direction. This optical access is more suitable for most practical application. It is appropriate to point out that since 90-degree scattering is rather weak, it is essential to minimize noise introduced by reflection of laser light on walls and optical components. The short recording distance also increases the efficiency of the laser energy utilization. To further increase particle image SNR, we reduce reconstruction aberration by in-situ reconstruction. This involves the use of both the same laser source and the same reference-beam optics for recording and reconstruction.

The high image SNR achieved by the off-axis configuration alleviates the need for de-noising in the data processing stage and thus greatly improves the overall processing speed. The high SNR also brings a highly efficient, yet simple implementation of a centroid finding algorithm. By utilizing only particle centroid locations instead of raw images, a compression ratio of several orders has been achieved. This allows the use of a fast concise cross correlation (CCC) algorithm, which works on particle centroids, thereby drastically improving processing speed over conventional cross-correlation.

In this paper we describe our new off-axis HPIV system developed in the Laser Flow Diagnostics Laboratory and show its preliminary applications in 3D turbulent and vortical flows.

3
System description

Based on the off-axis holography principle, we implemented a fully automated experimental off-axis HPIV, which employs 90-degree scattering, dual reference beams, in-situ reconstruction, and novel 3D data processing algorithms. At the core of HPIV data processing, a fast concise cross correlation algorithm for velocity extraction has been implemented, which works on particle centroids. The CCC process consists of correlation based on centroids and (optional) particle pairing. While correlation results are always statistical averaging of particle groups, by pairing individual particles in the correlation sets using the correlation results as a reference, super resolution (Keane et al. 1995) is achieved. The paired vectors are actually individual particle velocities, and the positions of these particles are already extracted through centroid finding. Such information on individual particles offers more possibilities for the applications of our off-axis HPIV technique. In this section we describe the HPIV system in detail.

3.1
Recording

Recording of particle images is the first step in HPIV measurement. Illustrated in Fig. 1 is the optical configuration for off-axis HPIV recording. An injection-seeded dual Nd:YAG laser (Spectra-Physics PIV-400) is employed, which gives a pair of temporally and spatially separated laser pulses, each of 8 ns duration, at a repetition rate of 10 Hz. Thus, the system is capable of double exposure to provide particle velocity measurement.

As in regular PIV applications, the double pulse separation Δt is adjusted according to the estimated flow speed. The two laser units contained in the dual YAG laser system are fired by a multi-channel digital delay generator. The addition of injection seeding to the standard PIV-400 laser guarantees sufficient coherence length (over a meter). The increased coherence length enables high-quality off-axis holographic recording of a large volume while allowing unmatched optical path lengths between object and reference beams. To ensure the stability of injection seeding operation, the pulsed laser system has to fire constantly during the recording process, and hence a pair of high-energy shutters operated through a synchronizer are

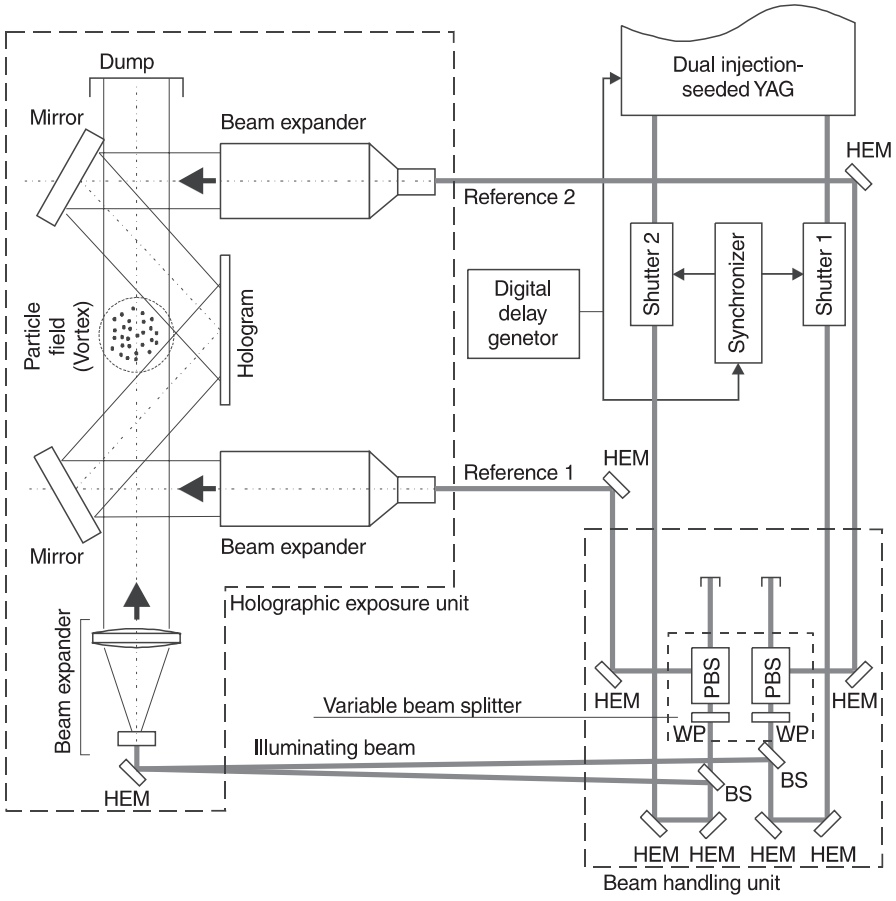

Fig. 1. Schematic of off-axis HPIV recording. Two laser beams from the injection-seeded dual YAG laser, separated by a short time interval, are splitted by the beam handling unit into 3 beams: The illuminating beam, reference 1 and reference 2. The holographic plate is placed with the emulsion side facing the particle field. A 3D region of the particle field is illuminated, and their 90-degree scattering is recorded on the hologram. *BS* Beamsplitter, *HEM* High Energy Mirror, *PBS* Polarizing Beamsplitter, *WP* Waveplate

needed to generate a single pair of laser pulses. The synchronizer assures each shutter to pass one and only one laser pulse each time.

Each laser head emits a beam, which, after passing through a shutter and a pair of high-energy mirrors (HEM), is split into two parts by a partial reflection mirror which works as a beam splitter (BS). The majority of the energy (80%) from each beam is reflected and used for illumination. The two illuminating beams, very close to each other, are combined at a common receiving HEM. The slight angular misalignment between the two beams becomes negligible after they pass through the illuminating beam expander. The transmitting part of each laser beam through the BS is further manipulated by a variable beam splitter (VBS), which consists of a pair of half-wave plates (WP) and a polarizing beam splitter (PBS). With the two VBS, it is possible to adjust the intensity of the reference beams and thus the reference-to-object intensity ratio. Evidently, the beam handling unit (enclosed by dashed line on the bottom-right corner of Fig. 1) produces three output beams: two separate reference beams (Reference 1 and 2) and one combined illuminating beam. It actually works as a multiplexer during double exposure: the illuminating beam is double pulsed, while the two reference beams are alternately single pulsed. This dual-reference-beam design provides angular separation of the reference beams for the double-exposure hologram, so that the two holographic images can be reconstructed alternately in time.

Three beam expanders are used to collimate the three beams and expand them into proper sizes: $3 \sim 5''$ diameter for the illuminating beam and $3''$ diameter for the reference beams. Since there is no special requirement on the quality of the illuminating beam, the beam expander needed is rather simple, consisting of a concave lens (for expanding) and a convex lens (for collimating). The two reference beams, however, should be high-quality plane waves for easy reproduction during the reconstruction (even with our in situ reconstruction, plane waves are preferred for producing conjugation beams). Hence, two factory-assembled beam expanders are used here. The reference beams are then bent over by a pair of flat mirrors to the holographic plate, which has its emulsion side facing the particle field (the flow region). The 90-degree scattered light from the particle field interferes with the reference beams, and the resultant interference pattern is recorded by the holographic plate. In this way a 90-degree-scattering dual-reference off-axis HPIV recording scheme is created.

Reference-to-object intensity ratio (R–O ratio) is one of the most crucial parameters in making successful holograms. In particle holography, where the object wave is a complex superposition of numerous weak near-spherical waves scattered by individual particles, R–O ratio plays an even more critical role. Both the R–O ratio based on individual scattering and the R–O ratio based on overall scattering intensity are important. First, it is the scattering from the individual particles that is responsible for forming the useful fringes on the hologram, hence the need

for appropriate R–O ratio based on individual particles. Second, the holographic film has a finite dynamic range for exposure energy. Since the film responds to the summation of the light energy at every point, the R–O ratio based on overall scattering intensity must be controlled. From a practical point of view, it is easier to work with the overall scattering intensity for the whole particle field since it is much more measurable and controllable than the scattering intensity of individual particles. Besides, its influence on film dynamic range is rather critical. The individual scattering R–O ratio has been found to have a rather high tolerance (Meng 1994), allowing some variations of the particle ensemble size under a given overall R–O ratio. For the range of the image volume ($1 \sim 3''$) and the seeding density we are currently interested in, an overall R–O ratio of 5:1 is found optimal in most cases. Understandably, its tolerance is closely related to the particle seeding density and image volume in the actual flow measurement.

3.2 Reconstruction

After the hologram is recorded and chemically processed, the 3D particle information contained within must be reconstructed – normally optically. To minimize aberrations so as to ensure high SNR, we reconstruct the holograms in situ, where exactly the same laser and the same reference beams used for recording are employed. This unconventional approach has proven very effective and convenient. As shown in Fig. 2, the hologram reconstruction system shares the same optics as the recording system, except that the object illustrating beam is blocked since it is no longer needed during reconstruction. The developed hologram containing interference fringes is now placed back at the original position, albeit with the film emulsion facing opposite to that of recording, such that each reference beam incident on the hologram becomes the complex conjugate of that used in recording. In this way, an unscrambled real image of the 3D particle field is reconstructed on the emulsion side, i.e. on the opposite side to the flow field.

The laser shutters are kept open at all times to pass every laser pulse for continuous hologram reconstruction and image acquisition. The two laser units are fired alternately, each at 10 Hz, to produce the two reference beams corresponding to those used for double-exposure recording. This way, the hologram alternately reconstructs the particle field recorded before and after the double exposure Δt.

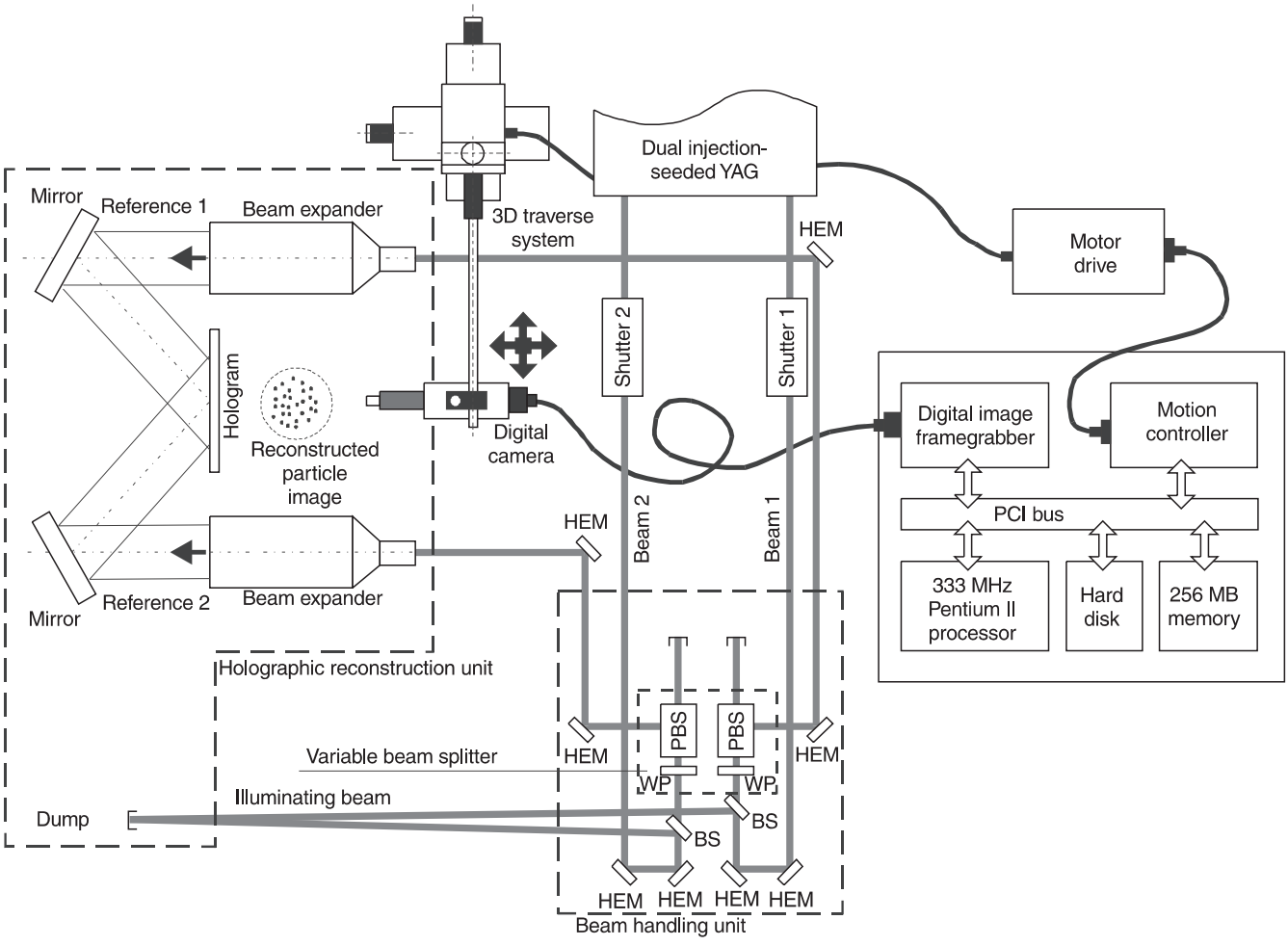

Fig. 2. Schematic of off-axis HPIV reconstruction (in situ). The hologram is placed at the original location where it is recorded, albeit with emulsion side facing opposite to the reference beam, forming a real image of the particle field on the opposite side. A computer controls the traversing system to move the digital CCD camera in three directions and acquire images plane by plane

Now that a frozen 3D particle field from each exposure is reconstructed continuously, it can be interrogated with a planar imaging device to be converted into digital form. A high-resolution digital CCD camera (KODAK ES1.0, 1 k × 1 k, 30 fps) mounted on a 3D traversing system (Daedal-Parker) is employed to capture the reconstructed holographic image. The camera sees only a small area of a thin slice at a time. The 3D image is interrogated slice by slice, and area by area. The entire particle field is thus decomposed into many 3D interrogation cells (IC), similar to the 2D interrogation spots (IS) in planar PIV. The pitch in depth direction, i.e. the distance between adjacent slices, must be small enough to resolve particle images along the depth direction. The IC size affects the processing speed and measurement accuracy, as well as the SNR of the acquired image. The choice of a larger IC size enables faster processing but also leads to a longer effective depth of focus of the particle image as seen by the CCD camera. This is because in order to increase the camera viewing area (zoom out), the effective N.A. of the objective lens on the CCD camera must be reduced. The increased depth of focus not only degrades measurement accuracy, but also causes interference of out-of-focus particle images, producing random spots or speckle noise. Therefore a compromise between the processing speed and the measurement accuracy is unavoidable.

In the current system data acquisition and processing are fully automated and controlled by a PC. A PCI digital image framegrabber is hosted in the computer to perform image capturing, and a motion controller is also installed to position the camera through the 3-axis traverse system. Image acquisition and camera movement are synchronized with the laser pulses to ensure data integrity. Data processing is completed on the fly, given that the processing is fast enough to follow the image acquisition and camera positioning. A speed of approximately one pair of image planes per second is achieved by the system.

4
Data processing

Figure 3 is a schematic diagram of data processing in our off-axis HPIV system. Digital images captured by the CCD camera are transferred into the system memory in the host computer via the framegrabber. The scanned 3D particle images contain a tremendous amount of data. Since the particle size and shape are not among the objectives of HPIV measurement, we compress the data into a list of particle centroid locations. To further obtain particle velocities, we correlate two particle centroid files corresponding to the two exposures made on the hologram using CCC algorithm, which consists of correlation and particle pairing.

4.1
Centroid finding

It is well recognized that the centroid finding process is the bottleneck of the processing speed since it is the data compression stage. Hence the centroid finding is critical to processing efficiency. Fortunately, because of the high image quality of the off-axis holography based on 90-degree particle scattering, no de-noising operation is needed in the centroid finding process.

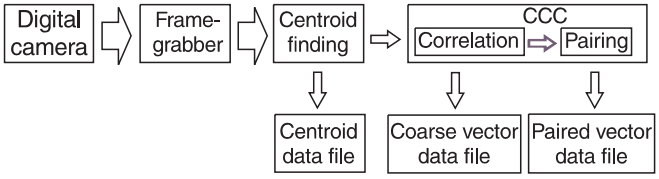

Fig. 3. Data flowchart during processing with concise cross correlation (CCC) and particle pairing

In the digitized image frames an image of a particle is a 3D cluster of pixels with high intensity. Since intensity peak of a particle image is typically located at its geometric centroid, a simple intensity-weighted-mean procedure (described below) provides the centroid location. The 3D centroid location coordinates are calculated according to:

$$x_c = \sum_{m=1}^{n} x_m I_m \Big/ \sum_{m=1}^{n} I_m$$
$$y_c = \sum_{m=1}^{n} y_m I_m \Big/ \sum_{m=1}^{n} I_m \qquad (1)$$
$$z_c = \sum_{m=1}^{n} z_m I_m \Big/ \sum_{m=1}^{n} I_m$$

where x_c, y_c, and z_c are the centroid coordinates, x_m, y_m, and z_m are the mth pixel in a 3D particle image, and I_m is its intensity, and n is the number of pixels in one particle image.

To extract centroids by applying Eq. (1), pixels making up the same particle images must be clustered, and noise pixels must be filtered out. This process consists of intensity thresholding and centroid computation, followed by further noise filtering based on 3D intensity summation of particle images. At first, an appropriate intensity threshold is set to separate particles from the background. Then a list of particle centroids is created and updated throughout the search in the image volume. Each element in the centroid list corresponds to a particle image, consisting of the 3D coordinates of the centroid and total intensity of the pixel cluster. During the process, the first pixel found above the intensity threshold becomes the first element in the list, and subsequently all other pixels in the image field are searched to build the centroid list. At any step, a pixel with intensity above the threshold is compared with other elements in the centroid list. If it is found to be in the proximity (within 8 pixels in x- and y-direction and 4 planes in z-direction) of an existing centroid in the list, it is considered a part of the same particle image. The data of this centroid is updated according to Eq. (1) to accommodate the new member in the cluster. If it is not in the proximity of any centroids, it is added to the list as a new particle centroid.

Even after the thresholding, the extracted centroid file may still contain noise, or false particles. This noise can be further reduced through CCC. We will show that CCC has certain tolerance to false particles.

As we perform image scanning and centroid finding, the energy of the laser beam to reconstruct the hologram often

fluctuates from pulse to pulse. This fluctuation is translated into intensity variation between interrogation cells and between different planes within the same 3D particle image, affecting the criteria of intensity threshold and thus affecting accuracy of particle centroids. To overcome this problem, we employ an adaptive threshold calculated based on the histogram of intensity in a plane that the CCD camera captures. Illustrated in Fig. 4 is a typical intensity histogram obtained from a plane in the reconstructed image. The particle images consist of pixels with high intensities, which appear to be a peak on the high intensity side of the histogram. Statistically they consist of an almost constant percentage of the whole image pixels. Since the laser pulse fluctuation has little effect on the profile of the histogram but only causes it to shift as a whole, we can set the intensity threshold at a certain percentage of the total pixels. Immediately after each image is acquired by the computer, its histogram is computed. The threshold is then calculated by counting pixels from the highest intensity down to the lowest side until a fixed percentage of pixels is included.

The accuracy of centroid locations is asymmetric along the three directions. In *x*- and *y*-directions (camera sensor plane) pixels are usually a few microns apart. In *z*-direction, however, sample points are on discrete image planes, whose pitch distance (between two adjacent planes) is typically 50–200 μm depending on the image depth of focus and desired data processing speed. Therefore the *z*-coordinate in the centroid finding requires a "sub-pixel" resolution for higher accuracy.

The uncertainties in finding particle centroids are the primary sources of error in the paired vector field. Therefore it is important to quantify such uncertainties. For this purpose we use simulated 3D particle images to examine the centroid extraction algorithm. In the simulations, numerically generated particles are randomly distributed in a given volume and projected onto a series of planes throughout the volume. The image planes are fed to the centroid finding algorithm. The extracted centroids are then compared with those initially generated particle locations to obtain the centroid errors in *x*-, *y*-, and *z*-directions. To obtain reliable statistical results, a large number of simulations have been performed.

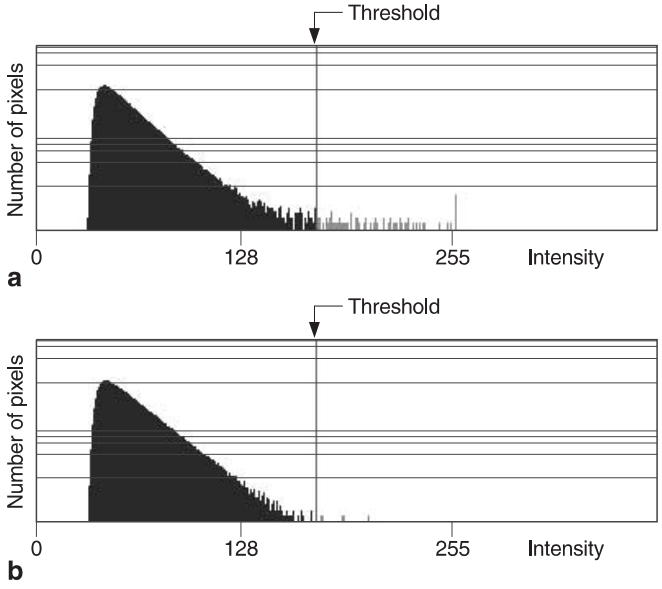

Fig. 4a, b. Intensity histogram of one acquired image plane in a logarithmic scale. **a** With particle images. There is a small peak at a high intensity value (255). Throughout the entire image volume, the percentage of pixels in such a peak is roughly constant. **b** Without particle images. The peak is absent

The simulations indicate that, uncertainty in *z*-direction is indeed much more severe than that in *x*- and *y*-directions. In general, *x*- and *y*-direction uncertainty is about 0.5 $\sim$ 1 CCD pixel distance, which translates into 2 $\sim$ 4 μm in our simulation. The *z*-direction uncertainty is approximately 0.2 pitch distance, or 18 μm at a pitch distance of 100 μm. Clearly, *z*-direction accuracy can be improved by reducing *z*-direction pitch; for example, the uncertainty drops to about 8 μm at a pitch distance of 50 μm. However, smaller pitch distance requires to process a larger quantity of image data. The uncertainties may also increase with the increasing particle density, because the chance of having agglomeration increases, which makes centroid extraction more prone to errors.

4.2
Concise cross correlation (CCC) algorithm

The essential part of CCC is the correlation, which will be discussed in detail first. Particle pairing after correlation will be discussed last.

Conventional FFT-based correlation has been the norm for velocity field extraction in planar PIV. For holographic PIV, where 3D velocity components are extracted in a 3D volume, it is generally assumed that this standard correlation method can be directly extended to 3D by either working with a 3D matrix (Gray and Created 1993; Huang et al. 1993) or two stereo 2D matrices (Barnhart et al. 1994; Meng 1994). Direct 3D FFT correlation appears impractical for high-resolution, large-volume off-axis HPIV measurement, since there are usually over 100 Gbytes of 3D image data per hologram, which, with FFT-based algorithms, can easily take thousands of hours to process. Furthermore, FFT-based correlation methods are effective only for high-density particle images and are thus prone to generating "bad vectors" in regions of low seeding densities (Meinhart et al. 1995). Unlike the case of planar PIV, HPIV deals with 3D volumetric recording, where the high seeding densities required for successful FFT-based correlation are difficult to achieve at an acceptable signal-to-noise ratio due to speckle noise. Hence, 3D FFT-based correlation is deemed unsuitable for our off-axis HPIV system. On the other hand, working with two stereo 2D matrices does provide relatively fast processing speed, but it suffers from an inherent low accuracy in depth direction and, more critically, requires a large viewing angle of the hologram to fit in two cameras. This often imposes difficulties on the holographic scheme.

We recognize that since only the displacements of particle images or at most their locations carry the information needed for velocity field measurement, it is unnecessary to store and handle the entire image data (which include redundancies such as particle sizes, shapes, intensities, background conditions etc.). Hence a correlation

procedure can be applied directly to the 3D locations of particles. This idea is implemented in the novel CCC algorithm, which yields a compression ratio of 4 to 5 orders and an increase in processing speed of 3 orders of magnitude.

The basic idea of CCC comes directly from the primary definition of cross correlation, whose physical meaning is image translation and multiplication/accumulation. Essentially, to cross correlate a group of particles in two exposures is to match the morphological patterns of the two images. The resemblance between the two patterns depends on the time interval between the two exposures and the velocity gradient of the flow. Therefore, the morphological deformation between the two patterns can be limited to an acceptable level by setting a small enough time interval. It is important to recognize that the correlation (pattern matching) procedure described above can be performed on particle centroid coordinates. Since most pixels in the acquired CCD image are dark background, the whole image data can be represented by a sparse matrix by taking all the particle centroids in the image as 1 and the background as 0.

The correlation works with two groups of particle centroids whose 3D coordinates are extracted from a pair of images in the double exposures. Keeping one of them fixed in its original place, we translate the other one in the 3D space and compute their correlation intensity. The displacement yielding the highest correlation peak is considered the displacement of the particle group and is the correlation output. Figure 5 illustrates how CCC works.

To quantify the probability of valid correlation results, or the "correctness", of CCC under various conditions, Monte Carlo simulations are performed. In correlating double exposures there are always particles in one group that do not have matching particles in the other group. We refer to them as "false" particles. Due to velocity gradients, the morphological patterns of the centroids also change between the two groups. The false particles and the morphological deformations are the major causes of invalid correlation. In the simulation we generate one group of centroids that are randomly distributed in a volume, then translate them by a given distance, individually shift each centroid by a small but random amount to mimic fluid deformation, and add a certain number of false particles to form the second group. Then CCC correlation is applied to these two groups of particles, and the correlation result is compared with the generated translation to validate the result. If the difference between the correlation result and the preset displacement is within one particle size, it is considered "correct".

Illustrated in Fig. 6a is the correctness of CCC as a function of the percentage of false particles. Performance under a wide range of densities (10 $\sim$ 270 particles per IC) has been simulated. In most cases with as many as 40% false particles the validity is still above 80%. Figure 6b shows the correctness of CCC as a function of morphological deformation. In the figure deformation is indicated as percentage of the IC size. It is found that satisfactory results can be obtained by CCC even at as high as 10% deformation.

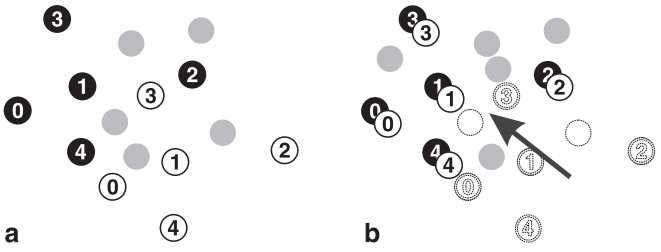

Fig. 5a, b. Principle of concise cross correlation (CCC). **a** Black and white balls represent two groups of particle centroids corresponding to two exposures. For illustration purpose they are numbered. Gray balls represent noise. **b** During the calculation, white balls and some of the gray balls are translated in 3D space, until their morphological pattern best matches that of the black balls

After CCC finds the mean displacements of particle groups, individual particles are paired to give individual particle displacements or super-resolution. In each Interrogation Cell, the first set of particle centroids is shifted towards the second by the mean displacement calculated from CCC. Now that there is no net displacement of the particle group but only net deformation between the two exposures, if the deformation is within a limit (as usually required by PIV), pairing can be accomplishable on the basis of the closest distance. Out of one IC, this pairing process produces multiple vectors corresponding to individual particles, achieving higher resolution and accuracy beyond correlation results. Theoretically, pairing process can produce hundreds of vectors out of one IC in contrast to FFT-based approaches, which produce only one vector out of one IC. Nonetheless, actual gain in spatial resolution depends on seeding densities used and quality of holograms. Large translational displacements of particle groups also reduce the number of particles that can be paired since some of them leave the IC volume.

The key elements of HPIV data processing can be summarized as follows:

- centroid finding provides large compression of image data,
- CCC (correlation) gives particle group velocities efficiently and reliably, and
- particle pairing provides super-resolution in velocity field.

5 Experimental results

5.1 HPIV measurement of a vortex ring in air

The off-axis HPIV system described above has been tested with measurement of a forced jet. Depicted in Fig. 7 is the experimental setup for the measurement of the vortex ring. The airflow, generated by a miniature electric fan, is seeded with water droplets 5 μm in size. It enters a chamber with a loud speaker mounted on the bottom and passes through a honeycomb, a contraction, and a circular nozzle. At 1-in. downstream of the jet exit, a vortex ring is

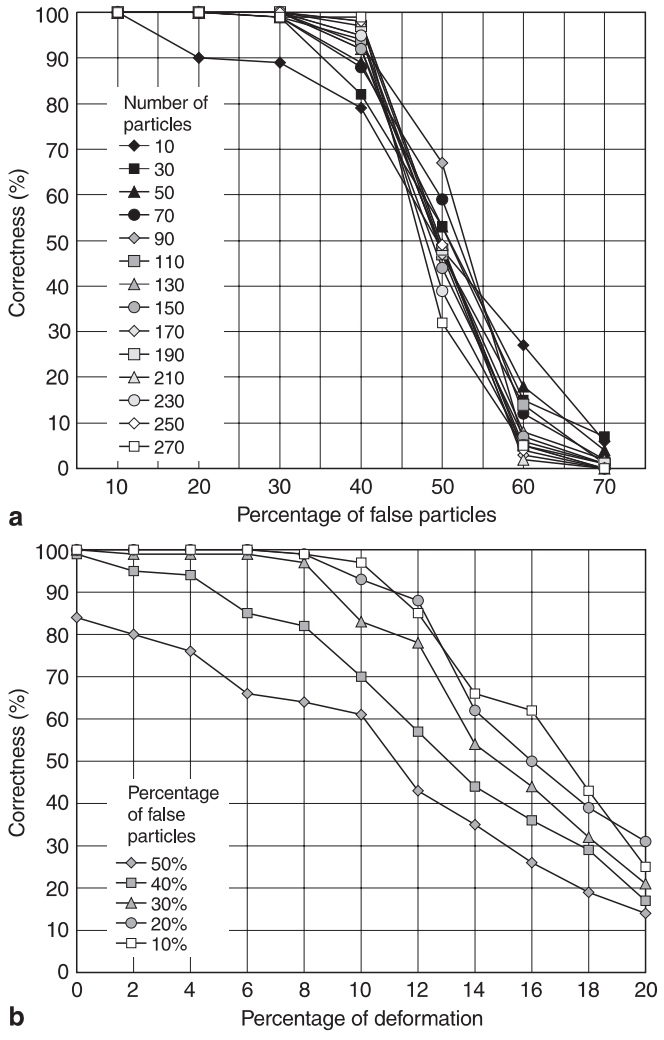

Fig. 6a, b. Correctness of CCC algorithm tested by simulation: **a** Correctness vs. percentage of false particles (noise) for various numbers of particles in a group. Average deformation is 2%. Note that with as much as 40% false particles the validity still reaches 80%. **b** Correctness vs. the amount of morphological deformation of the particle group for various percentages of false particles. The deformation is represented as percentage of the IC size

formed, which travels at ~2 m/s, corresponding to Re ~ 3400. The acoustic forcing is synchronized by a phase locked loop (PLL) with the 10 Hz laser pulses at constant (adjustable) phase delay, producing a stationary vortex ring located in the center of illumination. The dispersion of droplets in the 3D vortex ring is rather inhomogeneous, and the propagation of the vortex ring is unstable, as illustrated in Fig. 8a and b. The average seeding density in the vortex ring is approximately 30 particles per mm^3, which produces excellent image quality for data processing.

The R–O intensity ratio used to record the hologram is approximately 4:1. Depth of focus of particle images in this experiment ranges from 0.3 mm to 0.5 mm, for which a pitch distance of 100 μm is chosen for depth interrogation. A 4× microscope objective lens is mounted on the CCD camera to obtain a 2 × 2 mm viewing area, and with 20 image planes in each IC, the IC size is 2 × 2 × 2 mm. Therefore in the whole image volume, 50 (width) × 40 (height) × 50 (depth) = 12500 interrogation cells are acquired and processed, containing 250000 planar interrogation spots. With the CCD resolution of 1 k × 1 k, this corresponds to 250 Gbytes of data, which took approx. 50 h to process at the time of this measurement in 1997 (the speed has since increased by 7 times).

Shown in Fig. 8c are coarse 3D vector map in the flow volume extracted with CCC algorithm (correlation only). This instantaneous 3D snapshot of the test flow consists of approximately 6000 vectors. Only about 5% of the vectors produced by CCC are bad vectors, which can be easily identified and eliminated based on their lower correlation peak values. After cleanup of bad vectors, the residual bad vectors are well below 1%.

The 3D vortex ring structure can be identified from this preliminary 3D vector map. To increase spatial resolution, particle pairing is further performed on individual particles using the average vectors generated by CCC as references. More than 92,000 vectors are produced after particle pairing, gaining 15 times higher spatial resolution. The resulting raw velocity field is shown in Fig. 9, where the vectors are irregularly distributed in the 3D space. Since the particle distribution is inhomogeneous, at some test points there is no data.

From the dense version of the 3D velocity vector field, 3D vorticity field is calculated. To deal with missing data points and achieve higher accuracy, the velocity vectors are interpolated on a regular grid prior to the vorticity calculation. Illustrated in Fig. 10 is a vorticity iso-surface created from the computed vorticity field. It clearly depicts the 3D topology of the vortex ring measured.

5.2
HPIV measurement of a tab wake in a water channel

To test the feasibility of the HPIV measurement for water flows, off-axis HPIV technique is applied to a water channel flow with a tapered passive mixing tab mounted on the wall. The wake of such a tab is known to produce complex 3D vortical motions including a series of hairpin vortices (Yang et al. 1998; Yang and Meng 1999; Gretta and Smith 1993) and thus the tab is often called vortab. The free-stream flow velocity is approximately 16.7 cm/s, corresponding to Re ~ 12,000 based on the channel height and 2080 based on the tab height.

The holographic recording geometry of this flow is depicted in Fig. 11. The optical configuration is similar to the one employed in the air jet measurement. Hollow glass beads sized around 9 μm are illuminated by the volumetric laser beam at the test section. In this experiment, higher processing speed is achieved by adopting a large aperture objective lens with a low magnification. As a result the camera viewing area (and IC size) is increased to 4 mm × 4 mm and the processing time is reduced to 7 h.

Figure 12 shows a 3D snapshot of the velocity field measured in a volume of 44 mm × 56 mm × 32 mm composed of 9856 ICs. Around 80,000 paired vectors are produced, which is about 50% of the total number of particle centroids extracted. The low percentage of pairing is due to the large displacement between two exposures. The

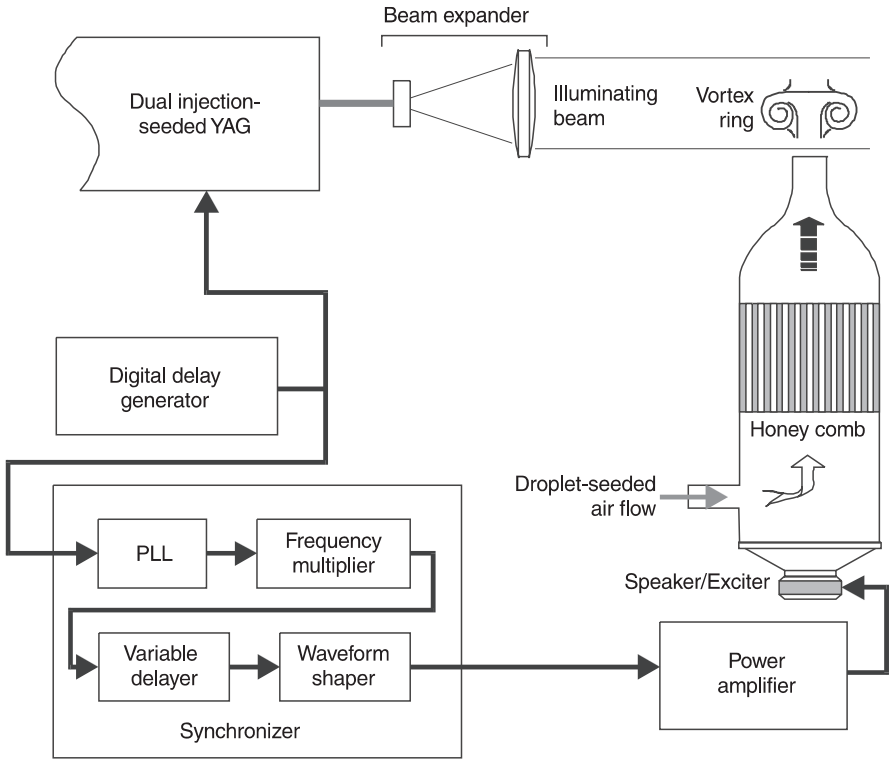

Fig. 7. Recording of a vortex ring in an air jet. The vortex ring is generated from an acoustically excited jet and synchronized with the laser pulse

paired vectors are gaussian-interpolated onto regular grids at 0.6 mm × 0.6 mm × 0.6 mm spacing, resulting in approximately 400,000 vectors. The gaussian radius used in the interpolation is 75% of the IC size. For clarity only those vectors on the outer surfaces are plotted, and the mean velocity averaged over all the vectors in the volume has been subtracted to make velocity gradients more visible. In the figure part of the volume is cut off to show the internal vortices. Coordinates X, Y and Z denote streamwise, wall-normal and spanwise directions, respectively. From this 3D velocity field, instantaneous vorticity field is computed to identify the hairpin vortex structure found in this flow using PIV (Yang et al. 1998; Yang and Meng 1999) and flow visualization (Elavarasan and Meng 1999). Shown in

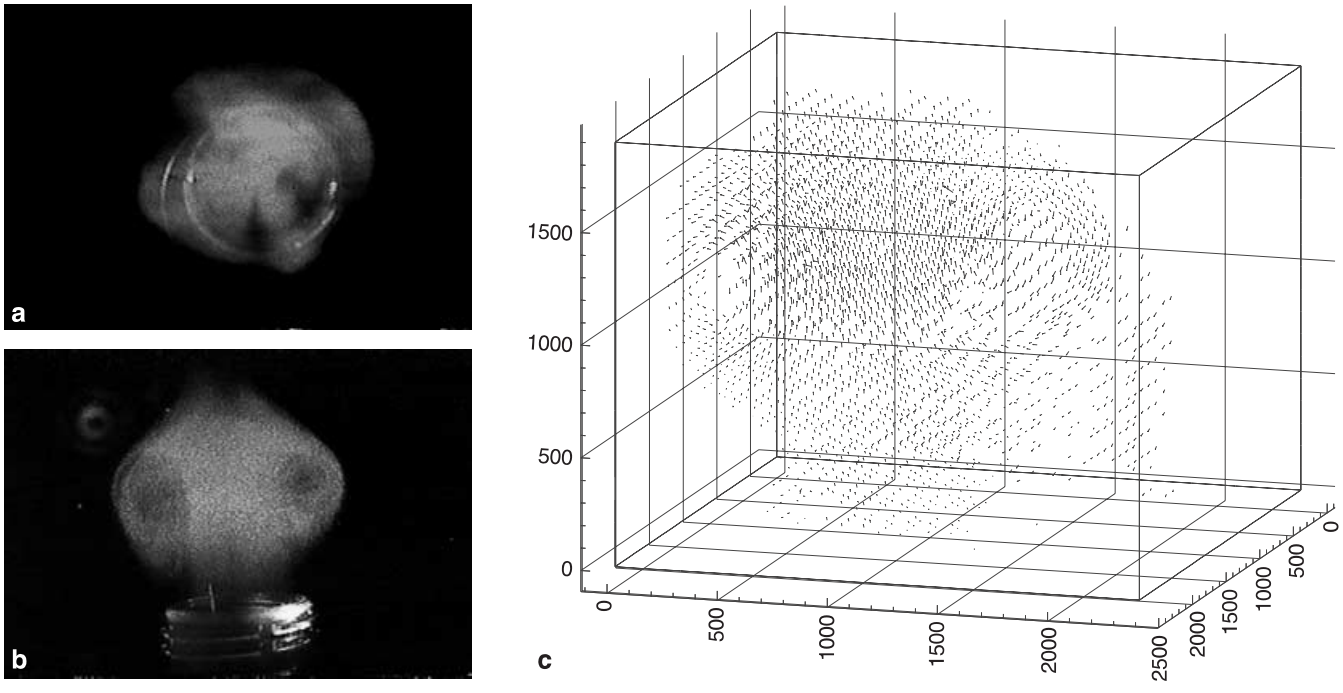

Fig. 8a–c. 3D vortex ring measured with HPIV. **a** and **b**: top view and side view photography. **c** Coarse 3D velocity vector field extracted from the hologram by CCC before particle pairing. Mean velocity of the jet has been subtracted from the result

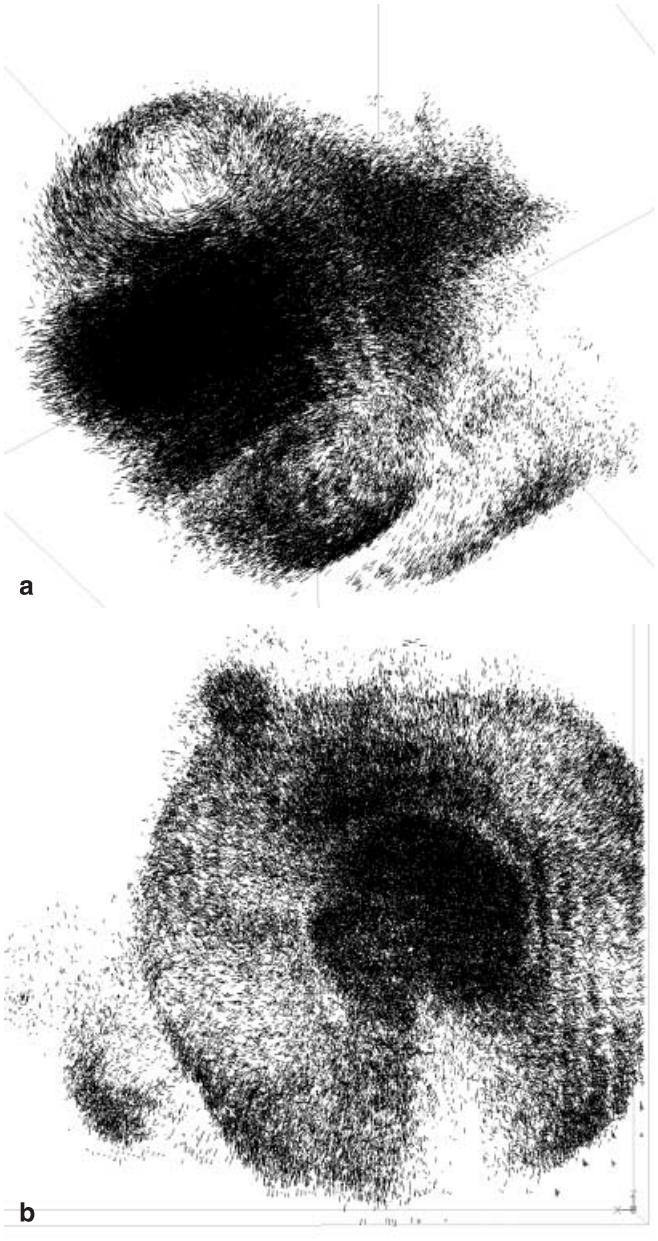

Fig. 9a, b. Detailed 3D velocity vector field after particle pairing: **a** side view. **b** top view. Approximately 92,000 velocity vectors are inhomogeneously distributed. A velocity vector field on a regular grid can be generated from this data by interpolation

Fig. 13 is an iso-surface of the vorticity field, where three hairpin vortices are identified in the 3D volume. Their size and streamwise spacing match those found by Yang et al. (1998). Such instantaneous 3D vortex structures, represented by vorticity magnitude, were only obtainable through numerical simulations before HPIV.

5.3 Result validation

The measurement accuracy of HPIV largely depends on the data processing. We have conducted a series of simulations to study the contributions of these factors. In this paper, however, we restrict our discussion to an evaluation

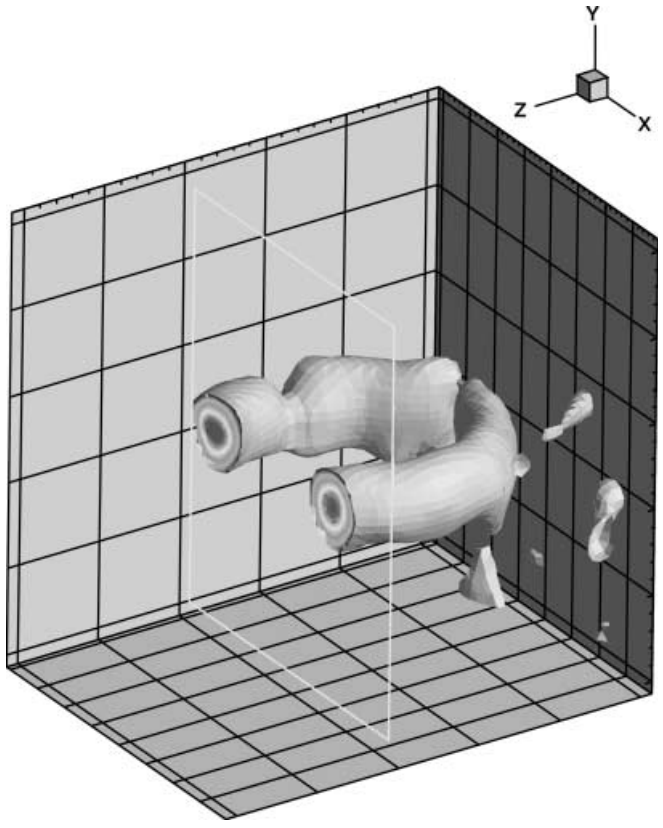

Fig. 10. Vorticity iso-surface calculated from the 3D velocity field of the vortex ring shown in Fig. 9. Part of the vortex ring is cut out to show the vortex core

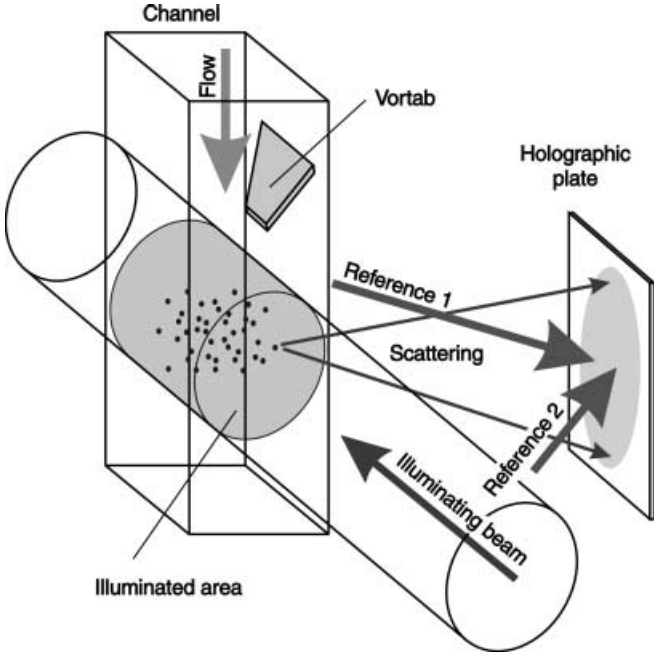

Fig. 11. Recording of the wake of a mixing tab in a water channel by using off-axis HPIV. The optical configuration is similar to that used in the vortex ring measurement. The free-stream velocity is approximately 16 cm/s

of the accuracy of our experimental results described in Sect. 5.2.

At first we examine what ultimately limits the velocity accuracy. Since the velocity field in Fig. 12 is derived from paired particles, i.e. the connection of particle centroids, uncertainty in centroid locations is the defining factor to measurement accuracy. During the data acquisition in this experiment, a plane pitch distance of 100 μm is employed. As mentioned in Sect. 4.1, this produces an uncertainty of approximately 18 μm in particle centroid. The mean displacements of particles extracted from the hologram are approximately 247 μm, or 61 pixels in the digital image plane (corresponding to a mean velocity of 16.5 cm/s with the double-exposure time interval of 1.5 ms used in the experiment). Therefore we estimate an overall velocity accuracy of no better than 7.3%.

Further validation of the experimental data is accomplished through examination of continuity equation. First, from the measured 3D velocity field, $\nabla \cdot \mathbf{u}$ (theoretically zero for the incompressible flow) is computed based on finite difference, whose probability density function (PDF) is depicted in Fig. 14. It is found that the divergence has a mean value of 0.51 s^{-1} and a standard deviation of 6.63 s^{-1}. The absolute value of divergence $|\nabla \cdot \mathbf{u}|$ has a mean value of 5.11 s^{-1} and 95% of data points are within divergence absolute value of 12.9 s^{-1}.

To provide a relative measure of error, we further resort to the mass conservation over an arbitrary control volume CV = $\Delta x \Delta y \Delta z$. The net flux entering the control volume is

$$\Delta Q = \iiint_{CV} \nabla \cdot \mathbf{u} \, dV \quad . \tag{2}$$

To estimate the order of the net flux, we introduce a characteristic velocity U, which is the main flow velocity in the flow field. The total flux passing through the control volume can be estimated as

$$Q = U \cdot \Delta y \Delta z \quad . \tag{3}$$

Therefore the non-dimensional ratio

$$\eta = \frac{\Delta Q}{Q} \tag{4}$$

provides an excellent indication of how well the continuity equation is satisfied.

For an estimation of the worst case, we choose the 95% coverage divergence value and the smallest control volume size (the grid size). In this case ΔQ is circa 2.78 mm^3/s. On the other hand, the mean flow velocity can be chosen as the characteristic velocity and Q is estimated to be around 59.0 mm^3/s. Therefore we estimate $\eta \sim 4.7\%$. Hence, continuity is satisfied reasonably well.

6 Discussions

The main purpose of HPIV is to measure full-field 3D flow velocity vectors. It is important to point out that, unlike conventional single-point measurements that rely on the temporal resolution to give information about turbulent flows, HPIV provides rich spatial quantitative information that no other quantitative experimental methods can provide. It directly probes into the 3D space. As such, HPIV provides a new way to tackle turbulence, providing instantaneous 3D flow structures, allowing for the application of coherent structures and construction of strain-rate tensor. These in turn provide new opportunities to understand turbulence and validate theoretical models.

Currently, our effort has been focused at increasing the information capacity (a combination of spatial resolution and measurement volume) and processing speed for in-

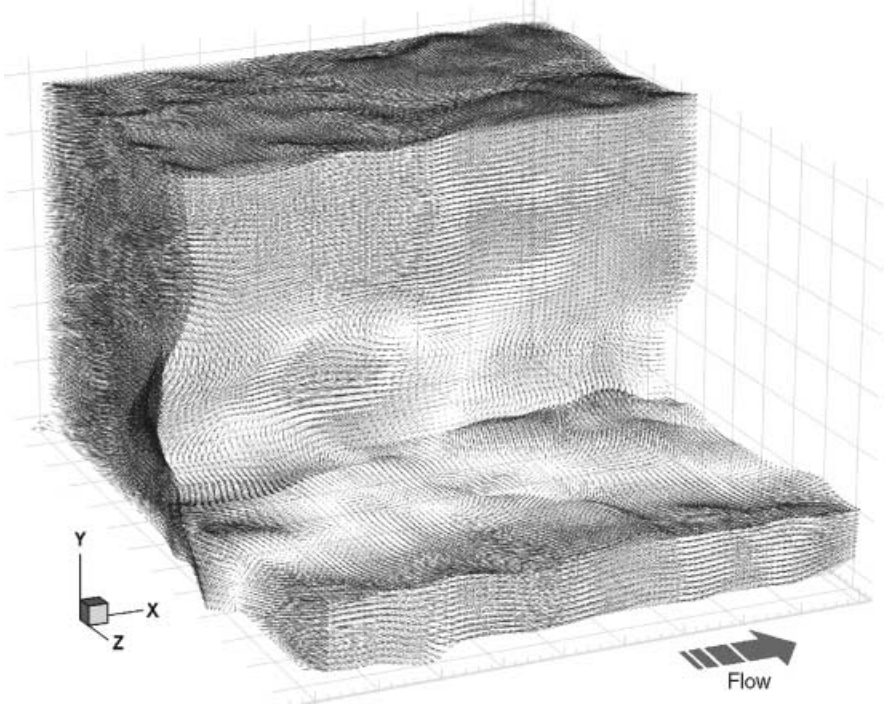

Fig. 12. An instantaneous 3D velocity field obtained from the tab wake obtained by HPIV. The measurement volume is 44 mm × 56 mm × 32 mm. Approximately 400,000 3D vectors have been gaussian-interpolated from about 80,000 paired vectors extracted by CCC with particle pairing. Mean velocity of the vectors has been subtracted and part of the measurement volume is cut out to show flow structures. For clarity, only surface vectors are shown

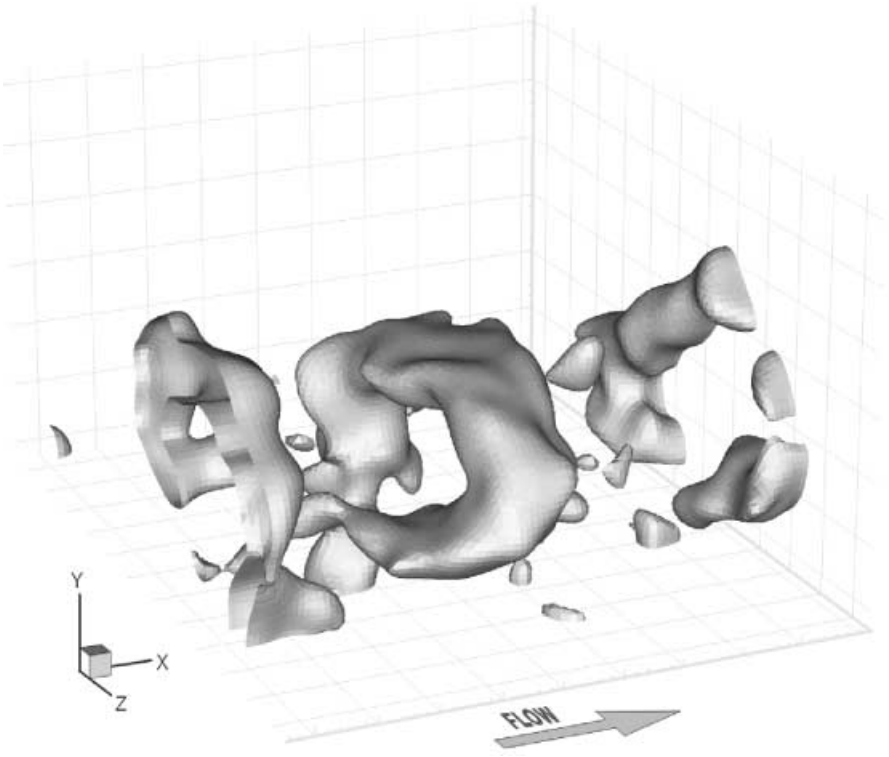

Fig. 13. Vorticity iso-surface obtained from the instantaneous velocity vector field in Fig. 12, showing three hairpin vortex structures

stantaneous HPIV realizations. When this stage of single-instant measurement becomes mature, the pursuit of cinematic HPIV will become sensible to obtain temporal resolution.

With the off-axis system described in this paper, the average particle seeding can reach as high as 50 per mm^3, yielding a spatial resolution (after particle pairing) of roughly 0.3 mm. The measurement volume, based on current size of the optics, is roughly 60 mm × 60 mm × 60 mm. Hence the largest-to-smallest length scale ratio of measurement is roughly 200. Further increase of the ratio can be achieved by scaling up the optics and, possibly, by increasing seeding density.

The dynamic range of the velocity measurement is determined by the ratio of 1/3 of the IC size (largest displacement allowed) and the particle centroid identification accuracy (the smallest displacement). By using a cascade procedure in data processing, the initial IC size can be rather large. The centroid accuracy is better than 4 μm along the transverse directions (perpendicular to the optic axis of image acquisition), but approximately twice as much along the axis with proper z-direction pitch distance and sub-"pixel" resolution. It is appropriate to estimate the typical dynamic range of velocity measurement as 500.

Besides 3D fluid velocity field measurement, HPIV can be used to diagnose particle position and velocity in multiphase flows. This is particularly straightforward with our off-axis HPIV technique, which preserves individual particle information. By using two types of particles with rather different Stokes numbers (one of them being much less than 1 and the other greater than 1), we can diagnose both the continuous phase and the discrete phase.

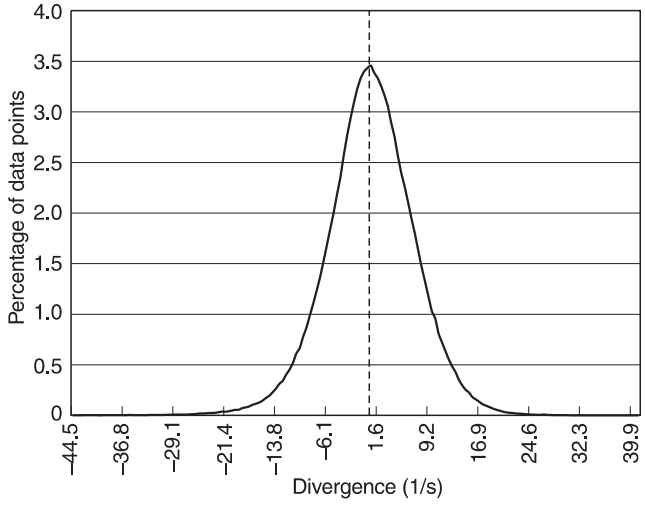

Fig. 14. Probability Density Function of divergence calculated from the 3D velocity field shown in Fig. 12. The mean of divergence is 0.51 s^{-1} and its standard deviation is 6.63 s^{-1}

7 Summary

In this paper we describe an advanced off-axis HPIV system with fully automated data processing. Its distinct features include the use of 90-degree scattering, dual reference beam recording, in situ reconstruction, on-the-fly processing, and a novel concise cross correlation (CCC) algorithm based on particle centroids. Our off-axis HPIV configuration offers superior image SNR at relatively high seeding density, alleviating the need for de-noising in data processing and enabling the use of CCC algorithm. A great gain on processing speed and data compression ratio is

achieved over traditional methods by using CCC. This innovative correlation approach also makes particle pairing possible, which greatly increases the spatial resolution. The off-axis HPIV technique has been successfully tested on two flows including an acoustically excited air jet seeded with water droplets and a surface-tab water channel flow. From both flows instantaneous 3D velocity fields are measured, from which vortex structures (a vortex ring and a series of hairpin structures) based on vorticity magnitude are obtained. Measurement accuracy is tested against continuity.

References

Adrian RJ (1991) Particle-imaging techniques for experimental fluid mechanics. Annu Rev Fluid Mech 23: 261–304

Adrian RJ (1996) Strategies for Imaging Flow Fields with PIV. AIAA 96-1988

Adrian RJ (1997) Dynamic ranges of velocity and spatial resolution of particle image velocimetry. Meas Sci Technol 8: 1393–1398

Adrian RJ; Soloff SM; Liu ZC; Meinhart CD; Lai W (1997) Stereoscopic PIV Applications to the Study of Turbulence. Workshop on PIV-Fukui, July 8–11, 1997, Fukui, Japan

Arroyo MP; Greated CA (1991) Stereoscopic particle velocimetry. Meas Sci Technol 2: 1181–1186

Barnhart DH; Adrian RJ; Meinhart CD; Papen GC (1994) Phase-conjugate holographic system for high-resolution particle image velocimetry. Appl Opt 33: 7159–7169

Belz RA; Menzel RW (1979) Particle field holography at Arnold Engineering Development Center. Opt Eng 8: 256–265

Bruecker Ch (1995) 3-D DPIV using a scanning light-sheet and stereoscopy: study of flow development around a spherical cap. ASME FED 229: 497–503

Bruecker Ch (1997) 3D scanning PIV applied to an air flow in a motored engine using digital high-speed video. Meas Sci Technol 8: 1480–1492

Cha S, et al (1993) Double-reference beam off-axis holographic particle image velocimetry. In: Holographic Particle Image Velocimetry, ed. E.P. Rood. ASME FED 148: 23–32

Elavarasan R; Meng H (1999) Flow visualization study of role of coherent structures in a tab wake, accepted by Fluid Dyn Res

Gray C; Greated CA (1993) Processing system for the analysis of particle displacement holograms, SPIE 2005, San Diego, pp. 636–647

Gretta WJ; Smith CR (1993) Flow structure and statistics of a passive mixing tab. J Fluids Eng, Trans ASME 2: 255–263

Guezennec YG; Zhao Y; Gieseke TJ (1994) High-speed 3-D scanning particle image velocimetry (3-D SPIV) technique. Proc Laser Symp, Lisbon, p. 26.1

Hinsch KD; Hinrichs H; Roshop A; Dreesen F (1993) Holographic and stereoscopic advances in 3D PIV. In: Holographic Particle Image Velocimetry, ed. E.P. Rood, ASME FED 148: 33–36

Huang K; Slepicka J; Cha SS (1993) Cross-correlation of three-dimensional images for three-dimensional three-component fluid velocity measurements. SPIE 2005: 655–666

Hussain F; Liu D; Simmons S; Meng H (1993) Holographic particle velocimetry: prospects and limitations. In: Holographic Particle Image Velocimetry, ed. E.P. Rood, ASME FED 148: 1–11

Keane RD; Adrian RJ; Zhang Y (1995) Super-resolution particle image velocimetry. Meas Sci Technol 6: 754–768

Meinhart CD; Adrian RJ (1995) Measurement of the zero-pressure gradient turbulent boundary layer using particle image velocimetry. AIAA 95–0789, Wash. DC

Meng H; Anderson WL; Hussain F; Liu D (1993) Intrinsic speckle noise in in-line particle holography. J Opt Soc of Am 10: 2046–2058

Meng H; Hussain F (1991) Holographic particle velocimetry: a 3D measurement technique for vortex interactions, coherent structures and turbulence. Fluid Dyn Res 8: 33–52

Meng H (1994) Development of Holographic Particle Velocimetry Techniques for Three-dimensional Vortical Flows. Ph.D. thesis, University of Houston, Houston, TX

Meng H; Hussain F (1995a) In-line Recording and Off-axis Viewing (IROV) technique for holographic particle velocimetry, Appl Opt 34: 1827–1840

Meng H; Hussain F (1995b) Instantaneous flow field in a circular vortex ring captured by innovative holographic particle velocimetry. Phys Fluids 7: 9–11

Meng H; Estevadeordal J; Gogeneni S; Goss L; Roquemore WM (1997) Holographic flow visualization as a tool for studying 3D coherent structures and instabilities. Proc 2nd Int Workshop on Particle Image Velocimetry. Viz Soc of Japan, Fukui, Japan, July 9–11

Prasad K; Adrian RJ (1993) Stereoscopic particle image velocimetry applied to liquid flows. Exp Fluids 15: 49–60

Scherer JO; Bernal LP (1997) In-line holographic particle image velocimetry for turbulent flows. Appl Opt 36: 9309–9318

Sheng J; Meng H (1998) A Genetic Algorithm approach for 3D velocity field extraction in holographic particle image velocimetry. Exp In Fluids 25: 461–473

Simmons S; Meng H; Hussain F; Liu D (1993) Advances in holographic particle velocimetry. SPIE 2005, San Diego, pp. 11–16

Thompson BJ (1974) Holographic particle sizing technique. J Phys E 7: 781–788

Trolinger JD; Belz RA (1973) Holography in dust erosion facilities. AEDC-TR-73–160

Weinstein LW; Beeler GB; Linderman AM (1985) AIAA-85-0526

Yang W; Sheng J; Meng H (1998) Study of Hairpin Vortex Dynamics and Turbulence Statistics of a Surface-mounted Mixing Tab Wake Using PIV. The 9th Int'l Symposium for Applications of Laser Techniques to Fluid Mechanics, Lisbon, Portugal, July 13–16, 1998

Yang W; Meng H (1999) Regeneration of hairpin vortices in the wake of a surface-mounted mixing tab, in preparation

Zimin V; Hussain F (1994) High-aperture raster holography for particle imaging. Opt Let 19: 1158–1160

Zimin V; Meng H; Hussain F (1993) An innovative holographic particle velocimeter: multibeam technique. Optics Letters 18: 1101–1103

Zhang J; Tao B; Katz J (1997) Turbulent flow measurement in a square duct with hybrid holographic PIV. Exp In Fluids 23: 373–381